Proceedings of the 28th IEEE
EMBS Annual International Conference
New York City, USA, Aug 30-Sept 3, 2006

Numerical Evaluation of Radio Frequency Power Deposition in Human Models during MRI

M. A. Stuchly, *Life Fellow, IEEE,* H. Abrishamkar, *Member, IEEE* and M. L. Strydom, *Member, IEEE*

***Abstract*—Concerns have been expressed about safety of MRI examination of two groups of people, namely pregnant mothers and cardiac pacemaker bearers. The main uncertainty relates to excessive heating by pulsed radio frequency (RF) fields. To address these issues, numerical evaluations of the power deposition are performed for a 27-week old fetus in a simplified model of the mother, and a realistic model of a human torso with an *in situ* pacemaker including its leads. The evaluations are supplemented with organ dosimetry for a realistic model of the human torso. An ideal non-resonant and two resonant birdcage coils operating at 64 MHz (corresponding to 1.5 T MRI) are evaluated. All simulations are performed with the finite difference time domain (FDTD) method.**

I. Introduction

One of the important research issues in MRI of humans is a potential for excessive heating of tissues due to radio frequency (RF) power. The problem is more pronounced for high magnetic field systems currently in use, typically 1.5 T. Even more concerns have been expressed regarding imaging of pregnant women and for patients with cardiac pacemakers. Only a limited number of investigations have been reported for imaging of the human torso [1]-[3], and none of the studies included a realistic model of a cardiac pacemaker *in situ*. Most of the evaluations of SAR have been performed for high-resolution models of human head. Furthermore, resonant birdcage coils, which are used in practice, have not been modeled because of computational challenges that they pose.

Heating due to RF fields is quantified in terms of the specific absorption rate (SAR) defined as:

$$SAR = E_i^2 \sigma / 2\rho$$

where: E_i is the electric field magnitude in tissue, σ is the tissue conductivity, and ρ is the tissue specific gravity.

Limits for the body average SAR and maximum value in 1 g or 10 g are prescribed in various guidelines and aimed at prevention of excessive tissue heating. The electric field can be computed in realistic models of the human body by numerical techniques, most often by the finite difference time domain method (FDTD) [4]. Alternatively, temperature increases can be measured in highly simplified models of the human body, which have homogeneous electrical properties.

Several investigations have been performed to determine SAR and/or temperature increases due to various implants [5]-[11]. Models of implants included simple metallic rods, as well as more realistic representations of actual devices. Two approaches to the evaluation of implants have been employed, namely numerical modeling and experimental measurements. Some studies used a realistic model of the human body or head, and simulated the electric fields with the FDTD method.

In this contribution, we present evaluation of the SAR in a heterogeneous model of the human torso and a 27-week fetus model due to exposure in birdcage coils at 64 MHz. The torso model contains a realistic model of the pacemaker placed in the left clavicle and the pacer lead treaded via the veins and terminating in the heart. Resonant and non-resonant configurations of the coil are modeled.

II. Models and Methods

A. RF Coils

Three coil configurations considered are: a non-resonant coil (representing ideal conditions – the best magnetic field uniformity) and birdcage resonators (used in practical systems). All coils have a diameter and a length of 0.7 m. The coils consist of sixteen equally spaced rungs forming a cylinder. Two circular rings are attached to the top and bottom of the open cavity. The non-resonant coil is excited in the midpoint of each strut with a progressive phase shift of 22.5^{O}. In the first resonant configuration, the capacitors are inserted in each strut. In second of the high-pass configuration, lumped capacitors are inserted in the ring at midpoints between the struts. This resonant coil is excited in 4 points equally spaced on one of the rings with a phase shift of 90^{O}. The 4 and 16-point excitations provide more uniform magnetic filed and are representative of the more modern systems.

B. Human Body Models

An anatomically realistic human model previously developed at the University of Victoria is used. This model is based on MRI images taken at 3.6 mm separations from a male of an average weight. The model is re-sampled to produce 5 mm resolution voxel size used in this work. The body model is composed of approximately 0.79 million cells. Over 30 distinct tissues are present, each with corresponding electrical properties at 64 MHz [12]. Table I summarizes these properties.

The female model is derived from MRI scans of a patient in her 27-week of pregnancy. The MRI data terminated

Manuscript received February, 2006. This work was supported in part by the Natural Sciences and Engineering Research Council of Canada (NSERC).

M. A. Stuchly is with the University of Victoria, ECE Department, Victoria, BC, V8W 3P6, Canada, and with the University of British Columbia, Vancouver, BC, Canada (e-mail: mstuchly@ece.uvic.ca).

H Abrishamkar was with the University of Victoria, ECE Department, Victoria, BC, V8W 3P6, Canada, (e-mail: houman@ece.uvic.ca).

M. L. Strydom was with the University of British Columbia, ECE Dept, Vancouver, BC, V6T 1Z4, Canada (e-mail: mstrydom@ece.ubc.ca).

abruptly above the groin and below the sternum. To avoid numerical artifacts caused by the termination, the model is extended with the same cross-section, to fill the computational domain. The pregnant female model consists of nine different tissues of which seven tissues types are inside the womb. The mother's body was assumed to be homogeneous, and having dielectric properties equal to two-thirds of muscle tissue ($\varepsilon_r = 48$ and $\sigma = 0.47$ S/m). The tissue permittivity inside the womb is derived from [13], which showed that the conductivity of tissue decreases significantly with age. The fetal properties were obtained by first finding the relevant tissue. The rest of the fetal properties were taken to be approximately two-thirds of muscle. Table II gives the properties of this model. Figure 1 the torso and fetus models placed in the birdcage coil, and Figure 2 illustrates the tissues of the fetus model.

TABLE I. ELECTRICAL PROPERTIES OF THE TORSO MODEL

Tissues	Dielectric Constant	Conductivity (S/m)	Density (g/cm^2)
Bladder	24.6	0.29	1.02
Blood	86.5	1.20	1.06
Bone	16.7	0.059	1.48
Bone marrow	16.4	0.15	1.08
Bowel	118	1.6	1.04
Brain	97.4	0.51	1.04
Cartilage	62.9	0.45	1.20
Colon	94.7	0.64	1.02
CSF	97.3	2.1	1.01
Fat	13.6	0.066	0.92
Gall bladder	105	1.5	1.00
Heart	107	0.68	1.03
Kidney	119	0.74	1.03
Liver	80.6	0.45	1.06
Lung	37.1	0.29	0.26
Muscle	72.2	0.69	1.04
Prostate/testes	84.5	0.89	1.04
Skin	92.2	0.44	1.10
Spleen	111	0.74	1.04
Stomach	85.8	0.88	1.04

TABLE II. ELECTRICAL PROPERTIES OF THE FETUS MODEL

Tissues	Dielectric Constant	Conductivity	Density
Amniotic fluid	114.6	10.0	1.01
Brain	114.6	0.67	1.03
Fetus	66.9	0.68	0.69
Kidney	162.0	1.01	1.03
Liver	93.9	0.57	1.06
Lungs	51.5	0.48	0.26
Mother	48.0	0.47	0.69
Placenta	80.0	1.00	1.06

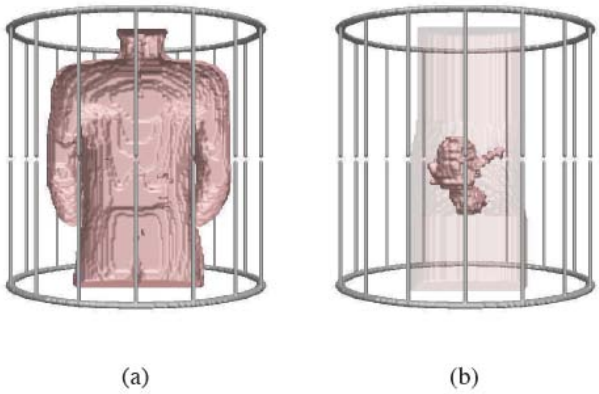

Fig. 1. Computational models in a birdcage coil: (a) torso, and (b) fetus

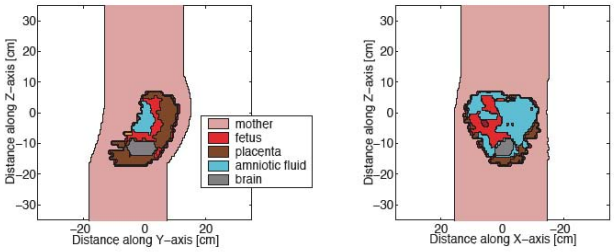

Fig. 2. Tissues of the fetus model.

C. *Numerical Method*

All computations are performed with the FDTD code with a spatial resolution of 5 mm. The computational space is terminated with 6 perfectly matching layers (PML).

The excitation source is the Gaussian pulse applied to specific components of the E field in the FDTD grid. The bandwidth of the pulse centered at 64 MHz is 30 MHz. Computations are run till a steady state is reached. All data are at 64 MHz using time-to–frequency transformation.

The pacemaker leads are modeled two different ways: as a perfect conductor and an imperfect conductor, both having a cross section of 5 mm square (equivalent to one FDTD cell) and a length of 0.37 m. The conductivity of the leads is determined based on measurements resistance of several leads and computation of the equivalent conductivity corresponding to the modeled cross-section, and it is equal to 148.5 S/m. Figure 3 illustrates the pacemaker model.

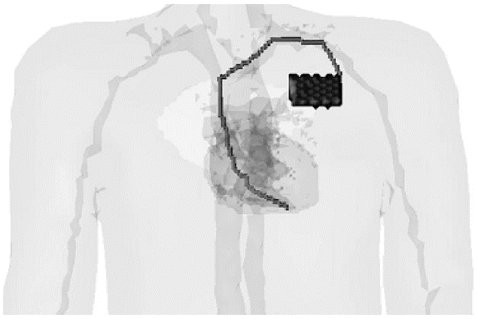

Fig. 3. Pacemaker inside the torso model.

III. Modeling Results

A. Organ Dosimetry: Adult

Table III summarizes organ dosimetry for the torso model in three birdcage coils considered. The data are for 1.957 μT in the center of the coil.

TABLE III. ORGAN AVERAGE AND 1 G MAXIMUM SAR

Tissue	Non-resonant		Resonant 16-point excitation		Resonant 4-point excitation	
SAR (W/kg)	Ave	1 g max	Ave	1 g max	Ave	1 g max
Blood	0.40	3.23	0.04	0.16	0.09	0.45
Fat	0.35	11.4	0.02	0.25	0.06	0.88
Heart	0.40	2.34	0.06	0.28	0.10	0.46
Kidneys	0.53	1.49	0.4	0.10	0.10	0.33
Liver	0.43	1.66	0.03	0.19	0.11	0.59
Lungs	0.10	3.74	0.01	0.48	0.01	1.25
Muscle	0.82	15.1	0.05	0.60	0.11	1.02
Skin	0.60	16.9			0.07	0.89
Stomach	0.48	4.37	0.07	0.16	0.09	0.33
Whole body	0.63	16.9	0.04		0.09	1.25

B. Organ Dosimetry: Fetus

Table IV gives organ average and 1-g maximum SAR values for the fetus model in the non-resonant coil and resonant coil excited in 16 rungs. The data are for 1.957 μT in the center of the coil.

TABLE IV. ORGAN DOSIMETRY FOR THE FETUS

Tissue	Non-resonant		Resonant	
SAR (W/kg)	Ave	1 g max	Ave	1 g max
Amniotic fluid	0.38	1.90	0.06	0.26
Brain	012	0.72	0.01	0.09
Kidney	0.15	0.26	0.02	0.04
Liver	0.08	0.47	0.01	0.11
Lungs	0.12	0.72	0.01	0.09
Placenta	0.36	1.20	0.05	0.17
Rest of the fetus	0.21	1.50	0.03	0.21
Mother	0.56	2.60	0.08	0.33

C. SAR Increase Due to Pacemaker

The increases in 1g SAR at the tip of the pacemaker lead are illustrated in Figure 4 and 5 for the two lead models. While the SAR enhancement patterns remain the similar for even for the two different coil excitations, the relative SAR increase is larger for the perfect conductor lead than the conductive lead in both coils. Numerical results are given in Table V.

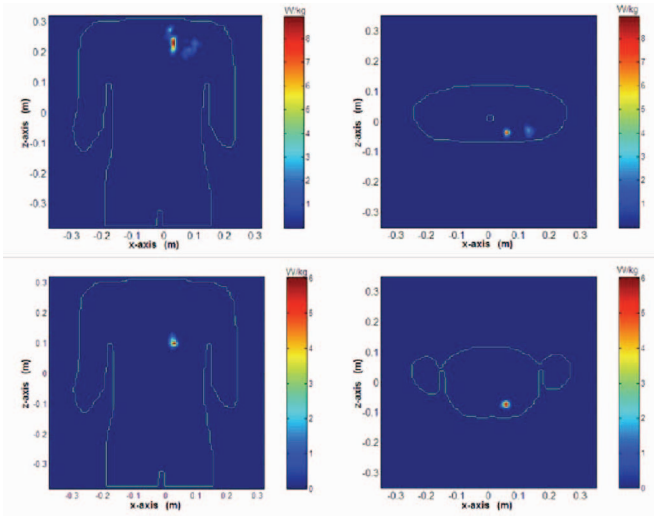

Fig. 4. SAR values (W/kg) averaged over 1 g tissue for the pacemaker model in the non-resonant coil for the perfect conductor lead: top row – the pacemaker generator; bottom row the lead tip (terminating at the heart).

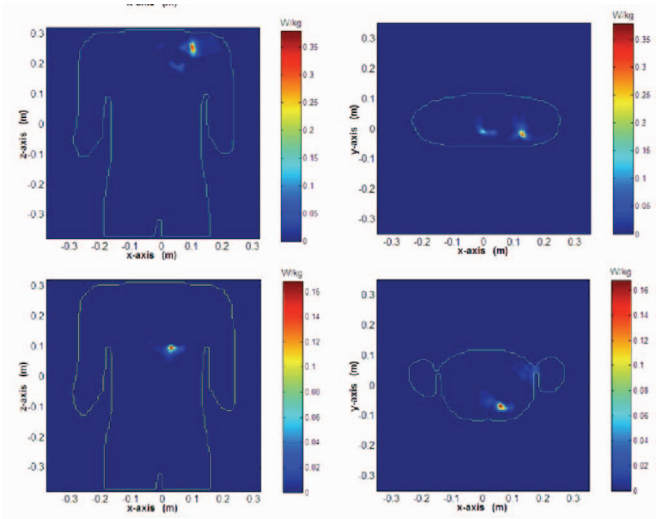

Fig. 5. SAR values (W/kg) averaged over 1 g tissue for the pacemaker model in the resonant coil for the conductive lead: top row – the pacemaker generator; bottom row the lead tip (terminating at the heart).

TABLE V. INCREASE IN THE 1G SAR VALUES (W/KG) DUE TO THE PACEMAKER LEADS AT THE GENERATOR END AND AT THE HEART

Coil	Non-resonant		Resonant	
Tip location	Generator	Heart	Generator	Heart
PEC	8.94	6.04	0.92	2.78
Conductor	1.17	0.56	0.38	0.17

IV. Discussion

There are few data in literature to which we can compare our results. Quantitative comparison of the average SAR values can be made with that in [1] for non-resonant coils, and as shown in Table VI the agreement is excellent considering differences in the torso models and placements and a difference in the coil dimensions (small).

TABLE VI. COMPARISON OF THE ORGAN AVERAGE SAR (W/KG)

Tissue	This study	Reference [1]
Blood	0.09	0.03
Heart	0.10	0.10
Kidney	0.10	0.11
Liver	0.11	0.16
Pancreas	0.05	0.06
Small intestine	0.14	0.15
Spleen	0.10	0.13

It can be clearly seen that much higher values of SAR occur in the non-resonant coil (Table III). This is consistent with the findings by others for the head coils, e.g. [13]-[14]. Also, lower SAR values are in the coil excited in 16 ports compared with the excitation in 4 ports similarly to the findings in [14]. In our investigation, the highest 1g SAR level in the non-resonant coil is observed in the skin at the periphery of the body in the high SAR region. Other high SAR values are detected nearby in the muscle and fat tissues.

In the case of the fetus, its SAR values are lower than those in the torso, as well as in the mother's body. This is a direct result of the highest SAR values occurring at or close to the body surface. Additionally, shielding of the fetus is produced by the amniotic fluid, which has high conductivity. While our model of the woman is highly simplified, its effect on the fetus dosimetry is expected to be limited.

In the case of the pacemaker, the numerical values of 1g SAR given in this work are for 5 mm diameter pacemaker leads. Thinner leads may result in higher SAR values. While typical leads have a diameter of about 5 mm, they consist of a much thinner wire wound as a helix. Based on the behavior of electromagnetic waves, the representation of the helix by a wire of the same cross-section and resistivity per unit length is expected to be correct in view of the small dimension of the wire compared to the wavelength (in tissue). There is however uncertainty regarding the dimension of the electrode terminating the lead, and a potential of higher SAR, id the electrode diameter is small.

V. Conclusion

The modeling performed and its comparison with the published data led to the following conclusions with respect to evaluation of the MRI safety for the pacemaker bearers in large birdcage coils operating at 64 MHz. The SAR in organs and SAR due to implants are overestimated for non-resonant coils excited in 16 rungs compared to practical coils employing resonant configurations. Typically, resonant coils produce SAR values that are about 10 times lower than those for non-resonant coils operating with the same magnetic flux density.

Cardiac pacemaker leads terminate in the heart, where the SAR values are relatively low, and thus the enhancement is relatively low. An evaluation of the SAR based on wires placed in the body periphery typically gives a large overestimate. Pacemaker leads are not perfect conductors, and modeling them as such, results in much greater 1g SAR than those produced by actual conductive leads.

Acknowledgment

The authors thank Dr. K Caputa of the National research Council Observatory in Victoria, BC, for his help with the models used in this study and Dr. P. Gowland of the Nottingham University for the MRI model of the fetus.

References

[1] P. Gandhi and X. Chen, "Specific absorption rates and induced Current Densities for an anatomy based model of the human for exposure to time-varying magnetic Fields of MRI," *Magn. Reson. Med.*, vol. 41, pp. 816–823, 1999.

[2] H. Ho, "Safety of metallic implants in magnetic resonance imaging," *J. Magn. Reson. Imaging*, vol. 14, pp. 472–477, 2001.

[3] C. Collins and M. Smith, "Spatial resolution of numerical models of man and calculated specific absorption rate using the FDTD method: A study at 64 MHz in a magnetic resonance imaging coil," *J. Magn. Reson. Imaging*, vol. 18, pp. 383–388, 2003.

[4] Taflove A, Hagness SC. Computational electrodynamics: the finite-difference time-domain method. Artech House: Dedham, MA., 1995.

[5] Smith, C.D., Kildishev, A.V., Nyenhuis, J.A., et.al., "Interactions of magnetic resonance imaging radio frequency magnetic fields with elongated medical implants," *J. Appl. Phys*., vol. 87(9), pp. 6188-6190, 2000.

[6] Chou, C.K., McDougall, J.A., and Chan K.W., "RF heating of implanted spinal fusion stimulator during magnetic imaging," *IEEE Trans. Biomed. Eng*., vol. 44(5), pp. 367- 373, 1997.

[7] Konings, M.K., Bartels, L.W., Smits K.F.M., et.al., "Heating around intravascular guidewires by resonating RF waves," *J. Magn. Reson.*, vol. 12, pp. 79-85, 2000.

[8] Nitz, W.R., Oppelt, A., Renz, W., Manke, C., Lenhart, M., Link, J., "On the heating of linear conductive structures as guide wires and catheters in interventional MRI," *J. Magn. Reson*, vol. 13, pp. 105-114, 2001.

[9] Park, S.M., Nyenhuis, J.A., Smith, C.D., et. al., "Gelled versus nongelled phantom material for measurement of MRI-induced temperature increases with bioimplants," *IEEE Trans. Magn.,* vol. 39(5), pp. 3367-3371, 2003.

[10] Shellock, F.G., "Metallic neurosurgical implants: evaluation of magnetic field interactions, heating, and artifacts at 1.5-Tesla," *J. Magn. Reson*., vol. 14, pp. 295-299, 2001.

[11] Achenbach, S., Moshage, W., Diem, B., et.al., "Effects of magnetic resonance imaging on cardiac pacemakers and electrodes", *Am. Heart J*., vol. 134(3), pp. 467-474, 1997.

[12] Gabriel, C., "Compilation of dielectric properties of body tissues at RF and microwave frequencies", Brooks Air Force Technical Report AL/OE-TR-1996-0037. Available:http://www.fcc.gov/fcc-bin/dielec.sh

[13] T. Ibrahim, R. Lee, B. Baertlein, et. al., "Application of finite difference time domain method for design of birdcage RF coils using multi-port excitation*", Magn. Res. Med*., vol.18, pp. 733-742, 2000.

[14] T. Ibrahim, R. Lee, B. Baertlein and P. Robitaille, "B1 field homogeneity and SAR calculations for the birdcage coil", *Phys. Med. Biol*., vol. 46, pp. 609-619, 2001.